Journal of Molecular Graphics and Modelling 27 (2009) 723–734

Contents lists available at ScienceDirect

Journal of Molecular Graphics and Modelling

journal homepage: www.elsevier.com/locate/JMGM

Homology modeling of human Transketolase: Description of critical sites useful for drug design and study of the cofactor binding mode

Cristian Obiol-Pardo, Jaime Rubio-Martinez *

Dept. de Química Física, Universitat de Barcelona (UB) and The Institut de Recerca en Química Teòrica i Computacional (IQTCUB), Martí i Franqués 1, E-08028 Barcelona, Spain

ARTICLE INFO

Article history:
Received 8 October 2008
Received in revised form 7 November 2008
Accepted 10 November 2008
Available online 19 November 2008

Keywords:
Transketolase
Homology modeling
Molecular dynamics
Binding free energy
Drug design

ABSTRACT

Transketolase, the most critical enzyme of the non-oxidative branch of the pentose phosphate pathway, has been reported as a new target protein for cancer research. However, since the crystal structure of human Transketolase is unknown, no structure-based methods can be used to identify new inhibitors. We performed homology modeling of human Transketolase using the crystal structure of yeast as a template, and then refined the model through molecular dynamics simulations. Based on the resulting structure we propose five critical sites containing arginines (Arg 101, Arg 318, Arg 395, Arg 401 and Arg 474) that contribute to dimer stability or catalytic activity. In addition, an interaction analysis of its cofactor (thiamine pyrophosphate) and a binding site description were carried out, suggesting the substrate channel already identified in yeast Transketolase. A binding free energy calculation of its cofactor was performed to establish the main driving forces of binding. In summary, we describe a reliable model of human Transketolase that can be used in structure-based drug design and in the search for new Transketolase inhibitors that disrupt dimer stability and cover the critical sites found.

1. Introduction

Transketolase is a cytosolic enzyme that catalyses the reversible transfer of two carbons, in a glycolaldehyde form, from a ketose donor substrate to an aldose acceptor substrate. It is also the most critical enzyme of the non-oxidative branch of the pentose phosphate pathway. This pathway provides ribose molecules that are an essential metabolite in nucleic acid production. In addition, the ribose necessary for the abnormal proliferation of tumor cells is provided via the non-oxidative branch of the pentose phosphate pathway [1]. In this regard, a metabolic control analysis gave a Transketolase tumor growth control coefficient of 0.9 [1]. Therefore, the inhibition of Transketolase could lead to the development of new anti-cancer drugs, which would decrease the rate of cell division and act at the most critical enzymatic step. Transketolase has also been proposed as a marker for Alzheimer's disease, due to its decreased activity in brain and other tissues of post-mortem patients [2].

Two studies [3,4] have shown that the mechanism of action of Transketolase is mediated by its cofactor thiamine pyrophosphate (TPP), which is coordinated to a divalent metal ion. However, drugs targeting the active site of Transketolase, and which act as cofactor analogs, have poor activity and low selectivity over other thiamine-dependent enzymes such as pyruvate dehydrogenase. oxythiamine [5] or thiamine thiazolone diphosphate [6] are typical examples of this kind of inhibitor, and thus they do not have any pharmacological application.

A lot of work has been devoted to yeast (*Saccharomyces cerevisiae*), *Escherichia coli* and maize Transketolases and their structures have been solved by X-ray diffraction [7–11], revealing important aspects of the functional flexibility, metabolic profile and substrate binding of these variants. Interestingly, three distinct domains were identified in yeast Transketolase: the N-terminal, middle and C-terminal domains [8,9]. The N-terminal domain (residues 1–322) contains the highly conserved TPP binding motif $GDG(X.X)_{25-30}N$, the middle domain (residues 325–538) contains a well-conserved sequence, specifically between residues 475 and 504, while the C-terminal domain (residues 539–680) has been implicated in the formation of a βαβ-fold, with an extended loop between the first β-strand and the α-helix.

However, little research has focused on the human Transketolase protein. A recent study of the human variant reported the critical importance of Asp 155, which is implicated in thiamine pyrophosphate binding [12]. In a similar vein, Du et al. [13] performed high-throughput screening on human Transketolase and found two inhibitors, with a new mechanism of action, but with an unknown binding site. Other authors have reported that some arginine residues (e.g. Arginine 433) are crucial for Transketolase stability

* Corresponding author. Tel.: +34 93 4039263; fax: +34 93 4021231.
E-mail address: jaime.rubio@ub.edu (J. Rubio-Martinez).

1093-3263/$ – see front matter © 2008 Elsevier Inc. All rights reserved.
doi:10.1016/j.jmgm.2008.11.005

and activity, although this was only identified for the rat variant [14]. More recently, a new class of thiamine analogs were designed as inhibitors of human Transketolase [15–17]. In this regard, it would be useful to determine the structure of human Transketolase in order to conduct further research into structure-based drug design. The present study therefore proposes the first model of human Transketolase, using the 3D structure of the yeast variant as a template and then performing a homology modeling which is subsequently refined through molecular dynamics simulations. This is a general strategy for obtaining a protein structure when no crystal structure is available, and it has been applied to several protein models with noteworthy results [18–20]. Moreover, the dynamic simulation is used to analyze the whole protein–protein interacting surface, which includes some hot spots containing conserved arginines, and to quantify the energetic nature of the thiamine pyrophosphate binding by applying the Molecular Mechanics Poisson–Boltzmann Surface Area (MMPB(GB)SA) protocol [21]. Experimental results [22] suggest that the fundamental interaction between the cofactor and the yeast protein is electrostatic, because a simple molecule of pyrophosphate can compete with TPP for the binding site, while the thiamine fragment of TPP does not compete. In this context, MMPB(GB)SA can provide interesting information, such as electrostatic and van der Waals energies, solvation energies and entropic contributions to binding.

2. Methods

2.1. Construction of the human Transketolase homodimer

The MODELLER 8v2 program [23] was used to construct the human structure. MODELLER is a general program that implements comparative protein structure modeling by satisfying spatial restraints in terms of probability density functions [24,25]. To this end, the homodimer crystal structure of the *S. cerevisiae* yeast Transketolase (pdb code 1AY0 [7]) was used as a 3D template. Although other variants, such as the *E. coli* Transketolase or the maize Transketolase show similar sequence identity to the human protein, the yeast variant was chosen because more information is available about its structure and properties.

Fig. 1 shows the sequence alignment between human and yeast Transketolases that is needed to perform the homology modeling. This was extracted from a multiple sequence alignment, including seven variants, reported by Sundström et al. [26]. The accuracy of the alignment is the most crucial step in assuring the quality of the homology modeling and a multiple sequence alignment is always the preferred approach.

Although the two proteins have low sequence identity (27%) the MODELLER program was applied to generate thirty satisfactory models for each monomer of human Transketolase. The model with the lowest energy and the lowest restraint violation was selected. As regards the secondary structure, STRIDE software [27] was used to predict secondary elements in both the yeast and the best MODELLER model of the human Transketolase (Fig. 1). The secondary structure of the model is similar to the yeast protein, thus confirming the quality of the homology modeling. The major differences are found in fragments containing gaps in the alignment; thus, the alpha helix between residues 269 and 279 in the yeast variant has no equivalent in human Transketolase. Moreover, the long alpha helix between residues 291 and 322 in yeast is constructed as two short alpha helices in the human variant because the alignment also has a gap in this region. These gaps are inevitable, since the human protein is 57 residues shorter than the yeast protein.

As regards the tertiary structure, Fig. 2 shows the two monomers with the best score for the human protein, superimposed over the crystal structure of the yeast variant. As can be

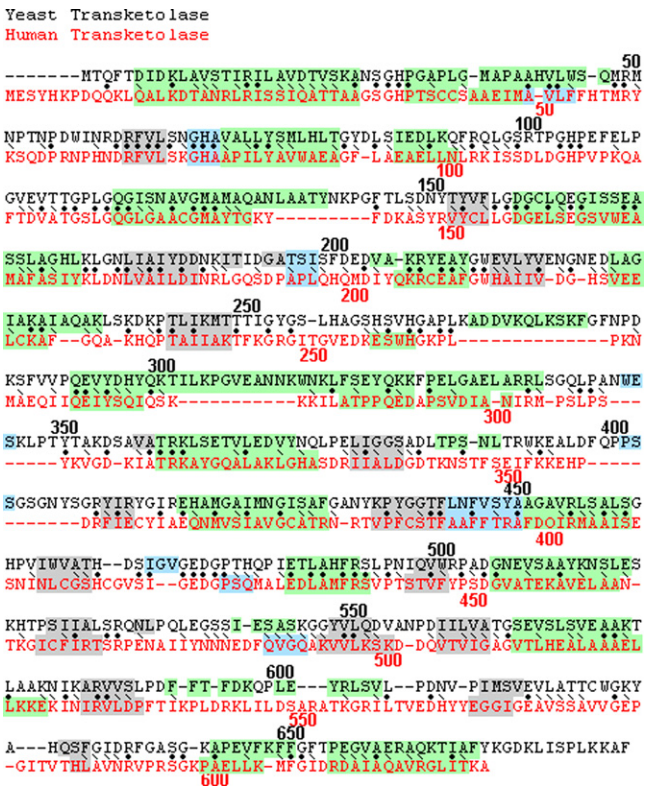

Fig. 1. Sequence alignment between yeast Transketolase (black) and human Transketolase (red) extracted from the multiple sequence alignment of Sundström et al. [26]. Conserved and similar residues are marked with a point and a left slash, respectively. Secondary structure prediction using STRIDE [27] is also shown. Alpha helices are shown in green, 3–10 helices are shown in blue and beta sheets are shown in grey.

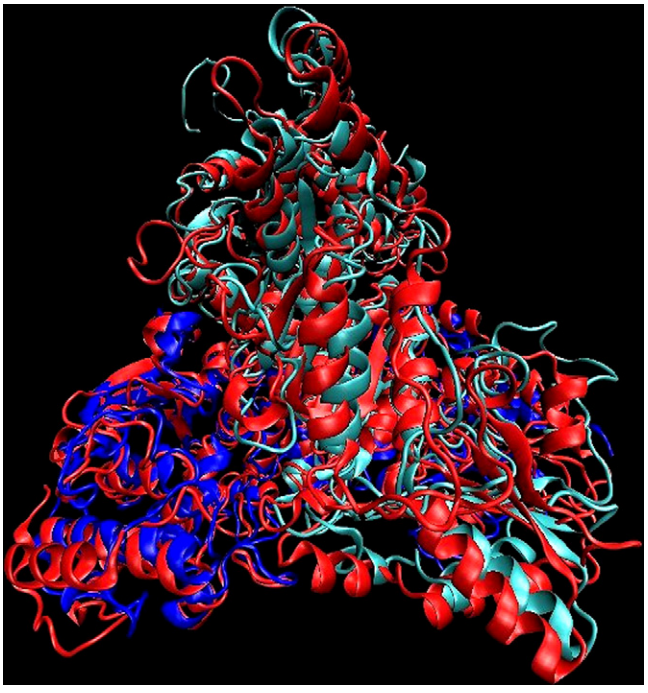

Fig. 2. Superimposition between crystal yeast Transketolase (red) and the two best MODELLER models of human Transketolase (best monomer 1 is shown in cyan, and best monomer 2 is shown in blue). Image created with the VMD software [34].

seen, the tertiary structure of both proteins is also very similar, providing a good starting point from which to refine the structure by molecular dynamics. To reveal the differences among the models, we compared the five MODELLER models with the best scores for each monomer of human Transketolase. Their backbone RMS deviations range between 0.8 and 1.1 Å. Only the two monomers with the best scores were selected to construct the homodimer (shown in Fig. 2) taking into account that a maximum deviation of 1.1 Å should be accessible for an usual molecular dynamics simulation. Finally, to better support our methodology, it was performed an additional homology modeling of human Transketolase taking the *E. coli* variant as template (pdb code 1QGD). The alignment between the two variants is also shown in Ref. [26]. The best scored models using both templates were superimposed. Both structures are very similar, showing a backbone RMS deviation of 1.9 Å, and this value decreases to 0.7 Å when we exclude the 10 disordered residues of both extremes. We therefore assumed that the modeling and refining of more than one initial structure from MODELLER or from related templates would be a redundant exercise in this system.

The dimer was constructed by imposing the same symmetry as that of the yeast Transketolase dimer.

In the second step the hydrogen atoms were added to the structure with the LEAP program of the AMBER-7 package [28]. Normal protonation states were applied, except for glutamic acid residues 157, 160 and 366, which were treated as protonated; this was also the case with the proposed protonation of the equivalent residues in yeast Transketolase [29]: Cys 159, Glu 162 and Glu 418, respectively.

The model was completed with the addition of the two TPP cofactors (superimposing their position and conformation from the yeast protein) and the two structural calcium cations coordinated to the pyrophosphate fragment of the TPP cofactors.

The AMBER force field parameters of thiamine pyrophosphate were calculated by the General Amber Force Field (GAFF) program [30] using a charge population derived from an adjustment to electrostatic potential (RESP) implemented in the GAUSSIAN-94 package [31].

Finally, a cubic box of approximately 26,300 TIP3P water molecules was added to the system to perform the molecular dynamics in an explicit solvent model, using periodic boundary conditions within the particle mesh Ewald (PME) context [32]. The system was neutralized by adding an appropriate number of counterions.

All calculations were carried out at the molecular mechanics level using the AMBER94 force field [33] with the AMBER-7 suite of programs [28]. All 3D figures in the present study were produced with the Visual Molecular Dynamics (VMD) package [34]. The pairwise RMS map shown in Fig. 3 was developed using the Chimera program [35].

2.2. Minimization and molecular dynamics

The human Transketolase dimer was energy-minimized to remove bad contacts derived from the homology modeling and to achieve a good starting structure with which to perform the molecular dynamics.

In the first step, of 1000 iterations, only water and counterion molecules were allowed to move. In the second step, of 1500 iterations, water and protein side chains were allowed to move. Finally 50,000 iterations were calculated with the restriction-free system up to an energy gradient of 1.71 kcal/mol.

The minimized structure was heated by coupling the system to a thermal bath at 300 K using Berendsen's algorithm [36] and at a constant rate of 30 K/10 ps; all atoms except water and counterions were maintained frozen. Time step was set to 2 fs and the list

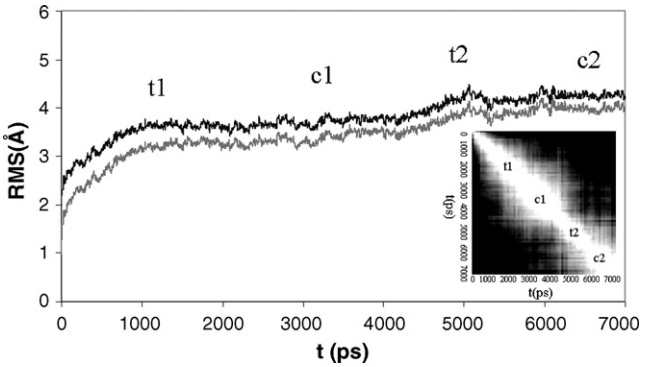

Fig. 3. Backbone RMS deviation of the human Transketolase model with respect to the initial structure (black) and the minimized structure (grey), versus time. First 13 nitrogen-terminal residues of both chains were not included in this analysis. The small box depicts the pairwise RMS map, showing transition zones (t1, t2) and stable structures (c1, c2). White represents structures with RMS lower than 2.0 Å, black represents structures with RMS higher than 2.8 Å and grey denotes for structures between both RMS values.

of nearest neighbor atoms was updated every 15 ps. A cut-off distance of 9 Å was chosen to compute non-bonded interactions and the SHAKE [37] algorithm was imposed in order to constrain all bonds involving hydrogen atoms.

Once the system was heated a second step of 40 ps at constant pressure was calculated to increase the density of the system. The restrictions on solute main chains and cofactors were then relaxed gradually until the system was free. Finally, 7 ns of molecular dynamics were calculated within the NVT ensemble at a constant temperature of 300 K.

2.3. Binding free energy calculation

The MMPB(GB)SA protocol [21] was applied to calculate the binding free energy of the cofactor (TPP) in complex with the human Transketolase model. This protocol was used within the one-trajectory approximation, and computes the binding free energy as follows:

$$\Delta G_{\text{binding}} = G_{\text{complex}} - (G_{\text{receptor}} + G_{\text{ligand}}) \quad (1)$$

$$G = E_{\text{MM}} + G_{\text{Polar Solv}} + G_{\text{Non-Polar Solv}} - \text{TS} \quad (2)$$

$$E_{\text{MM}} = E_{\text{int}} + E_{\text{vdw}} + E_{\text{ele}} \quad (3)$$

$$G_{\text{Non-Polar Solv}} = a\text{SASA} + b(\text{for the PB contribution}) \quad (4)$$

$$G_{\text{Non-Polar Solv}} = c\text{SASA}(\text{for the GB contribution}) \quad (5)$$

where E_{MM} denotes bond, angle and dihedral force field energies, and E_{vdw} and E_{ele} are the van der Waals and electrostatic energies. $G_{\text{Polar Solv}}$ is the polar contribution to solvation, calculated in a continuum medium using the MEAD software [38] and solving the linear Poisson-Boltzmann equation (PB). An external dielectric constant of 80 was set to treat the system with solvation. Additionally, the generalized born methodology [39] was also applied to solve the polar contribution, using the parameterization of Tsui and Case [40], denoted in this work as GB1, and the parameterization of Onufriev et al. [41], denoted in this work as GB2. This latter calculation requires the use of the bondi radii set [42], while GB1 contributions were calculated using the parse radii set [39]. PB contributions were calculated using both sets of radii.

Finally, $G_{\text{Non-Polar Solv}}$ is the non-polar contribution to solvation, related linearly with the solvent accessible surface area (SASA), while a takes the value of 0.00542 kcal/mol Å^2 and b the value of

0.92 kcal/mol. To calculate this contribution in the GB context, c takes the value of 0.0072 kcal/mol Å^2.

SASA was computed by means of the Linear Combination of Pairwise Overlap (LCPO) method [43]. Entropic effects were computed through a normal mode analysis using the nmode module of AMBER-7. The Minimization step before normal mode analysis was carried out up to an energy gradient of 10^{-4} kcal/mol.

MMPB(GB)SA was applied to 100 equidistant snapshots extracted from the production time, except for the entropic contribution, which is computationally intensive, and therefore is usually based on only a few snapshots. For this contribution, 10 snapshots were extracted by limiting the system to only those residues located at a distance of 9 Å from the TPP cofactors.

3. Results

3.1. Stability and assessment of the model

To verify the stability of the model, we examined the total energy of the system versus time; last 1.6 ns were considered as the production time, once the total energy was stabilized. In addition, the backbone RMS deviation of the full system from both the initial and minimized structures is shown in Fig. 3. Average RMS deviations were 4.0 and 3.6 Å, respectively, which can be considered as a measure of the quality and stability of the model. Energy and RMS convergence was achieved after more than 5 ns of molecular dynamics, due to the slow conformational changes of side chains together with the low sequence identity of the two variants. As can be seen, a long molecular dynamics is necessary to improve the initial MODELLER structure, and in general, it is required to refine a homology model with low sequence similarity. To investigate structural changes along the molecular dynamics, a pairwise RMS map is also shown in Fig. 3. This analysis was used to identify similar structures that were stable throughout the simulation. We identified two zones with stable structures, named c1 and c2, between two zones of transition, named t1 and t2. Average structures were extracted from c1 and c2 and compared. Unsurprisingly the most important differences were found in N-terminal and C-terminal fragments. However, the sequences Pro 263 to Gln 272, Asp 339 to Ser 345 and Glu 349 to Lys 353 have no defined structure in c1, although these sequences do have some tertiary structure (alpha helices) in c2. In summary, the Transketolase structure improved throughout the molecular dynamics simulation, when the total energy and RMS deviation were stabilized.

As regards the cofactor, the all-atom RMS deviation of the first TPP is shown in Fig. 4 (similar results were obtained for the second TPP). There is also a small fluctuation throughout the simulation, in agreement with a good binding site description. Average RMS deviation of TPP with respect to the initial structure (extracted from the yeast variant) was 1.1 Å, while the value was 1.4 Å with respect to the minimized human structure. In this case the minimization structure is not as representative as the initial one, thus through the dynamics simulation the TPP conformation becomes closer to the conformation in yeast, which is the bioactive conformation of TPP, and presumably, also the conformation for the human variant.

To verify the symmetry between the two Transketolase monomers they were superimposed to evaluate the final molecular dynamics structure. Backbone RMS between monomers was 2.8 Å. This is also a small deviation, revealing a close similarity between the two subunits.

As a final test of the quality of the model, the PROCHECK [44], Verify-3D [45] and ProSA [46] programs were used. The former was applied to quantify the residues in available zones of the Ramachandran plot, selecting the MODELLER model of human Transketolase. Thus, 82.5% of residues were located in the most favored zones, 14.2% in allowed regions, 2.2% in generously allowed regions, and 1.1% (14 residues) in disallowed regions. Similar results were obtained for the final molecular dynamics structure. Verify-3D uses a score function to assess the quality of the model. Fig. 5 shows the Verify-3D profile for the final molecular dynamics structure; residues with a score over 0.2 should be considered reliable. Thus, 73% of residues have a score over 0.2 for monomer 1 and 79% for monomer 2. Fig. 5 also shows that the sequence between residues 250 and 300 exhibits lower scores. This fragment corresponds to a sequence of the human protein that includes two gaps in the alignment (Fig. 1) [26]; however, this fragment is solvent exposed, with no role in dimer stability or cofactor binding. In future studies, therefore, we do not intend to focus on this modeled fragment. Finally, Fig. 6 shows the energy profiles for the MODELLER model and for the final molecular dynamics structure using the ProSA score. This program evaluates the energy of the structure using a distance-based pair potential. Residues with negative ProSA energies confirm the reliability of the model. In addition, as can be inferred from Fig. 6, the molecular dynamics simulation improves the results of the ProSA energy, by decreasing the number of residues with positive peaks (Fig. 6C and D).

3.2. Description of dimerization sites involving arginine residues

Eight structures (one each 200 ps) of the Transketolase model along the production dynamics were used to identify the most relevant protein–protein interactions. We focused on the important residues for protein–protein recognition. In this regard, Hu et al. [47] found that arginine is the second most common residue

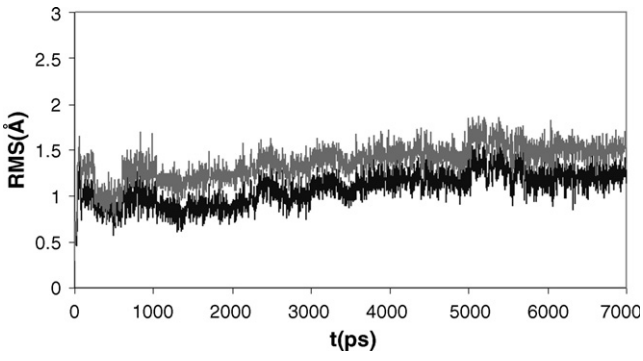

Fig. 4. All-atom RMS deviation of TPP with respect to the initial structure from yeast (black) and the minimized human structure (grey).

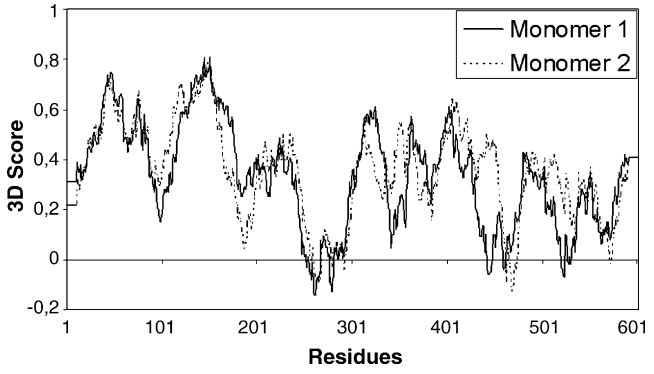

Fig. 5. Verify-3D score profile calculated for both monomers of human Transketolase and for the final molecular dynamics structure. Scores over 0.2 indicate a high quality model.

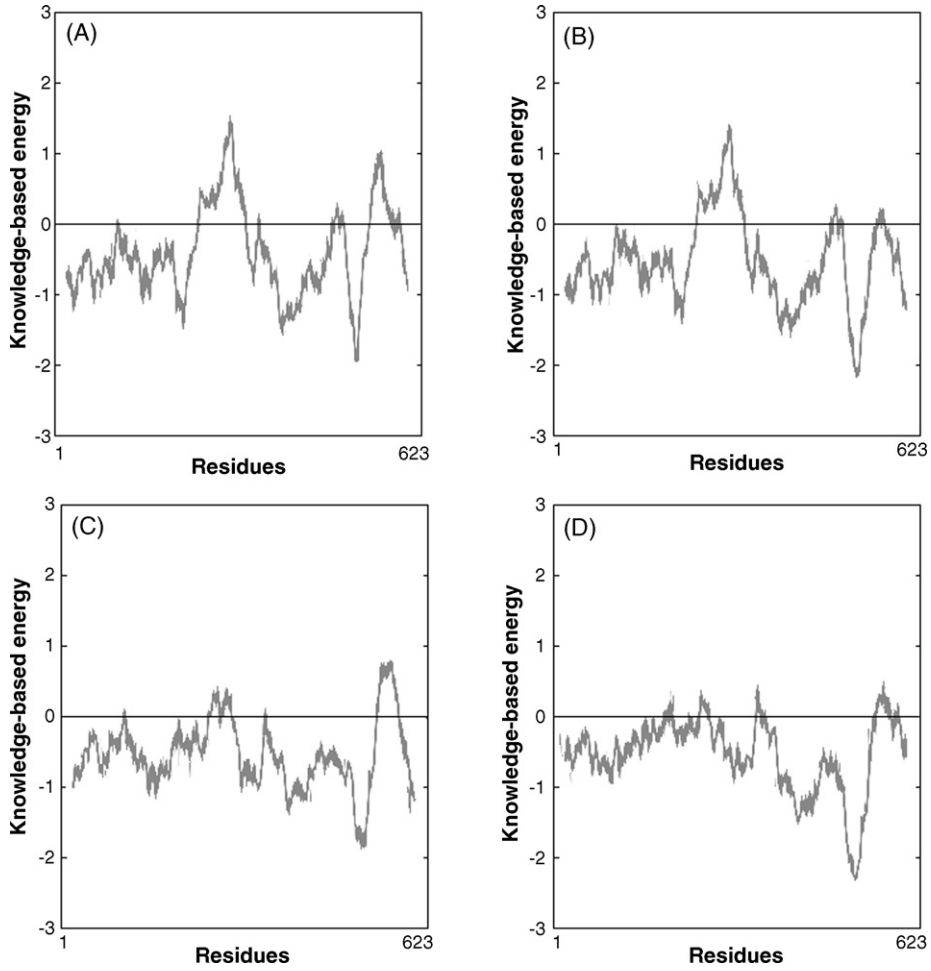

Fig. 6. ProSA energy profiles. A: Monomer 1 and MODELLER structure. B: Monomer 2 and MODELLER structure. C: Monomer 1 and final molecular dynamics structure. D: Monomer 2 and final molecular dynamics structure. Negative scores indicate a high quality model.

configuring hot spots and the first in terms of conservation propensity. In addition, Kremer et al. [48] showed that one arginine per monomer, at an unknown position, is essential for enzymatic activity of Transketolase. Later research by Soh et al. [14] identified four conserved arginines of rat Transketolase as being important residues for protein stability and catalytic activity.

Given these results we used our homology model to search for hot spots containing arginine residues in order to obtain the corresponding findings for human Transketolase. These sites would be exploited in order to design an interface inhibitor of human Transketolase. As pointed out earlier, this kind of inhibitor could be more interesting than a cofactor derivative. Moreover, several compounds have been designed with an arginine or an arginine analog to enhance their activities [49], and disruption of protein dimers by using small molecules has also been reported [50,51].

Table 1 shows four conserved arginines (Arg 102, Arg 350, Arg 433 and Arg 506) which are important for the catalytic activity of rat Transketolase, as demonstrated by site-directed mutagenesis (arginine to alanine mutation) [14], and their equivalent residues in yeast and human variants. Interestingly, replacement of Arg 433 by alanine in rat Transketolase was found to reduce protein activity dramatically [14]. Here we used our model of the human protein to investigate the role of the equivalent arginine residues, Arg 101, Arg 318, Arg 401 and Arg 474.

Thus, eight structures (one each 200 ps) from the production dynamics of the human model were extracted and contacts of conserved arginine residues were analyzed. To this end, hydrogen bond, van der Waals and electrostatic energies were calculated between all the arginine residues of the first monomer and all the residues of the second monomer. This methodology can be used to determine the most important sites (hot spots) for protein–protein recognition. Table 2 gives the distance and angle parameters of the hydrogen bond found. Only Arg 101 and Arg 401 maintained hydrogen bonds with the other monomer (the most important being with Asp 424 and Glu 432, respectively). Both bonds are formed by charged residues (also called salt bridges). In addition, we found another residue, non-conserved Arg 395 (which corresponds to Tyr 448 in yeast Transketolase), which also forms stable intermolecular hydrogen bonds.

As regards Arg 318 and Arg 474, it has been suggested [52] that their respective residues in the yeast variant (Arg 359 and Arg 528) are involved in substrate binding. They did not establish any intermolecular hydrogen bond throughout this simulation and therefore they are not directly involved in dimer stability.

Table 1
Conserved arginine residues from yeast, human and rat Transketolases. Reduced enzymatic activities of mutations to alanine in rat Transketolase are shown in brackets.

Yeast	Human	Rat
R94	R101	R102 (R102A, full activity)
R359	R318	R350 (R350A, 36.7%)
R454	R401	R433 (R433A, 6.1%)
R528	R474	R506 (R506A, 37.0%)

Table 2
Geometrical parameters of the intermolecular hydrogen bond found involving conserved arginines throughout the simulation.

Monomer 1	Monomer 2	Average distance (Å)	Distance RMS (Å)	Average angle (°)	Angle RMS (°)
Arg 101 NH2-HH21	Asp 424 OD1	1.9	0.2	151.0	10.6
Arg 101 NE-HE	Asp 424 OD1	2.1	0.3	144.8	10.3
Arg 395 NH2-HH21	Asp 398 OD2	3.2	1.1	143.1	17.5
Arg 395 NE-HE	Asp 398 OD1	2.5	0.8	153.7	11.3
Arg 395 NH2-HH12	Glu 160 OE2	2.3	0.5	136.7	17.1
Arg 401 NH2-HH22	Glu 432 OE2	1.9	0.2	153.4	11.5
Arg 401 NH1-HH12	Glu 432 OE1	2.3	0.4	144.3	1.0
Arg 401 NE-HE	Ala 391 O	2.3	0.5	133.3	22.6

Non-conserved Arg 395 is also shown.

As a complement to this analysis Fig. 7 shows the intermolecular van der Waals and electrostatic force field energies of each arginine residue described, as well as that of Arg 395. As can be seen, and consistent with the hydrogen bond pattern, Arg 101, Arg 401 and Arg 395 exhibit high interactions, specifically the electrostatic energy, which ranges between −36.2 and −55.1 kcal/mol, while the van der Waals energy ranges between −4.6 and −10.4 kcal/mol. However, the absolute value of these contributions cannot be compared directly. Electrostatic forces that can be considered as responsible for long-distance recognition are always decreased by a desolvation effect, while van der Waals forces are related to mutual volume recognition suffering a low desolvation effect. With respect to Arg 318 and Arg 474, they do not interact with the other monomer, as shown in Fig. 7.

As a further complement to this discussion about critical arginines, Fig. 8A–D show the close environment (around 9 Å) of these arginine residues. Fig. 8A shows the close environment around Arg 101. This residue forms a salt bridge with Asp 424 of the other subunit (shown in blue) and also maintains some contacts with the same chain (shown in cyan). Although Arg 101 is close to TPP it does not interact with the cofactor and, moreover, it does not interact with residues involved in the cofactor binding site. Corroborating this, mutation of Arg 101 in rat Transketolase does not affect the activity (Table 1).

Fig. 8B shows the environment around Arg 318 and Arg 474, which do not make any contact between monomers but, rather, form salt bridges with Glu 476 and Asp 424 of the same monomer (shown in cyan).

As was pointed out earlier the same two residues in yeast are involved in substrate binding and, therefore, their mutations to alanine decrease the activity of Transketolase by directly affecting the reaction compounds. Our model does not contain the reaction substrate to demonstrate this, but the two arginines are close to each other, with a favorable disposition for the substrate molecule bound between both residues.

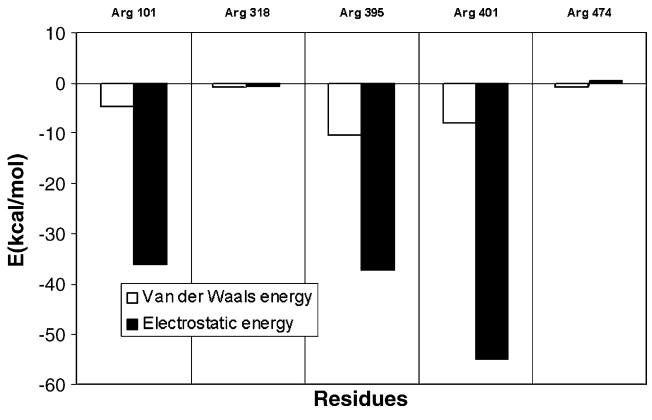

Fig. 7. Average intermolecular van der Waals energies (white bars) and electrostatic energies (black bars) of five selected arginine residues.

Fig. 8C represents the closest residues around Arg 395, which we suggest is important for dimer stability. This arginine forms an intermolecular salt bridge with Asp 398 (chain in blue) and it is also close to the carboxyl group of Glu 160 and the carbonyl group of Gln 367. Based on our model we argue that an alanine replacement of Arg 395 would be unfavorable for dimer stability and, therefore, for human Transketolase activity.

Finally, Fig. 8D shows the contacts of Arg 401 (equivalent to Arg 433 in rat Transketolase). The mutation to alanine was found to decrease enzyme activity dramatically. It should be noted, in line with the analysis of rat Transketolase, that this arginine is also the most critical residue for the human variant. First, it maintains the most energetic electrostatic interaction (−55.1 kcal/mol, Fig. 7) with the other monomer, with Glu 432 being the most affected residue. Second, Arg 401 is in close contact with a conserved sequence, V^{419}SIGEDGPSQMALE^{432}, called conserved loop, which maintains direct interactions with the TPP cofactor. The Gln 428 enclosed in this sequence is equivalent to the critical His 481 of yeast, which is involved in the activation of TPP. Moreover, Arg 401 is close to Phe 389 and Phe 392; the former interacts by π–π stacking with the aminopyrimidine ring of TPP. This is also shown in Fig. 8D. Thus, the alanine replacement of this residue could distort dimer stability and the TPP binding site at the same time and, therefore, its mutation to alanine should exhibit the most important effect, as occurs in the rat variant.

Concluding these analyses, we propose five human Transketolase sites containing arginine residues which could be explored to design an interface inhibitor, especially covering the site centered on non-conserved Arg 395 and conserved Arg 401. The Arg 101 site seems to be secondary, while the Arg 318 and Arg 474 sites may require substrate modeling to design an inhibitor that mimics this zone.

Interestingly, Arg 401 belongs to an alpha helix domain with the sequence F^{397}DQIRMAAISES^{408} (Fig. 8D, shown in cyan). Designing peptidomimetics of alpha helices is a well-known strategy in drug design. One of the most widely applied alpha helix analogs is the family of substituted biphenyls [53]. In this context, it may be possible to design a substituted biphenyl analog of this alpha helix sequence which contains the critical Arg 401 in order to disrupt the Transketolase dimer and inhibit its activity.

3.3. Description of dimerization sites using the MMGBSA protocol

Although no experimental data have been reported for non-arginine residues involved in the stability of the Transketolase dimer, other dimerization sites can be identified to search for new inhibitors that could bind to the monomer-monomer interface. To verify this, an MMGBSA 'per residue' protocol [54] was applied to calculate the binding free energy of all residues of monomer 1 with respect to the whole second monomer. This was done using the parameterization of Tsui and Case [40] (GB1). Thus, the most important residues should show the strongest interactions in the dimer interface. Moreover, this methodology describes not only

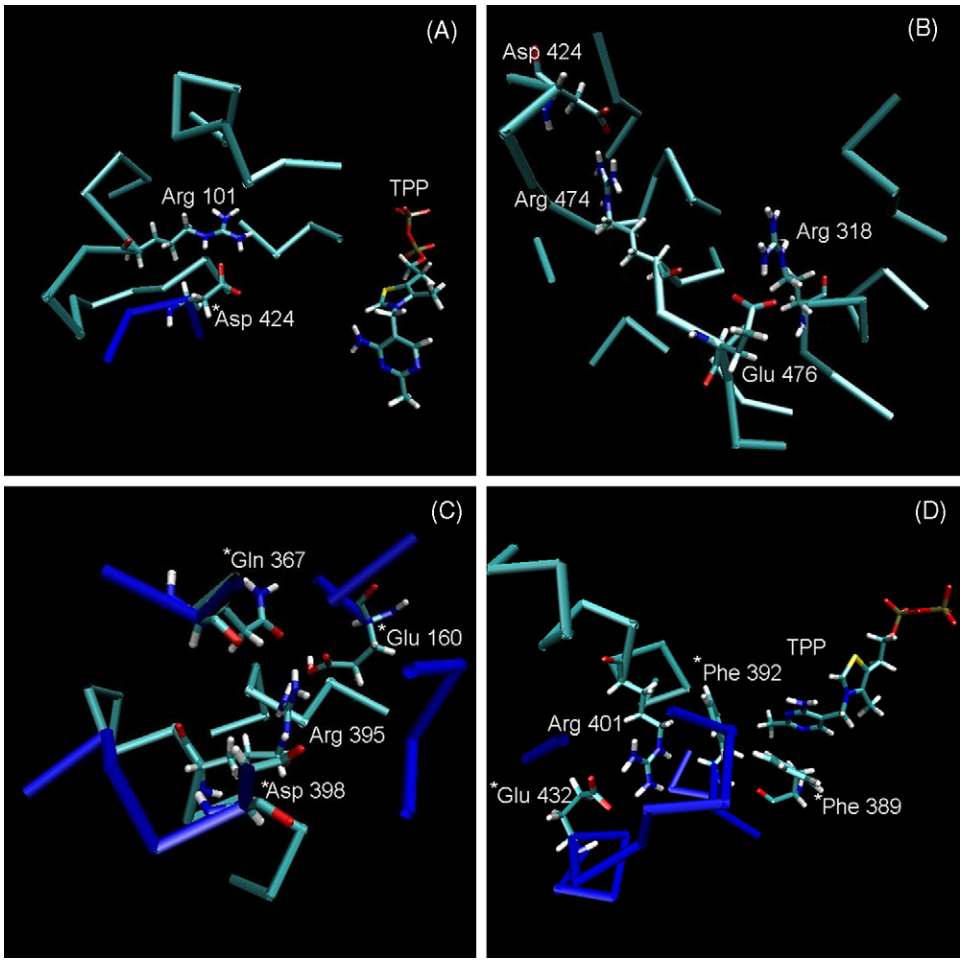

Fig. 8. Environment around 9 Å around selected arginine residues, Arg 101(A), Arg 474 and Arg 318 (B), Arg 395 (C) and Arg 401 (D). Water molecules not included. Monomer 1 is coloured cyan while monomer 2 is coloured blue. Residues of monomer 2 are marked with asterisks. It is also shown the disposition of the TPP cofactor, in A and D. Images created with the VMD software [34].

the interactions 'in vacuo' but also the solvation contribution to the final binding free energy. Fig. 9 shows the results of this analysis, plotting the ΔGB_{TOT} contribution (which includes van der Waals and electrostatic interactions, polar solvation contribution and non-polar solvation contribution) versus each Transketolase residue of monomer 1. Also included are the cofactor (TPP), the structural metal and a structural water which are discussed in the next section. It can be seen that the binding between subunits is

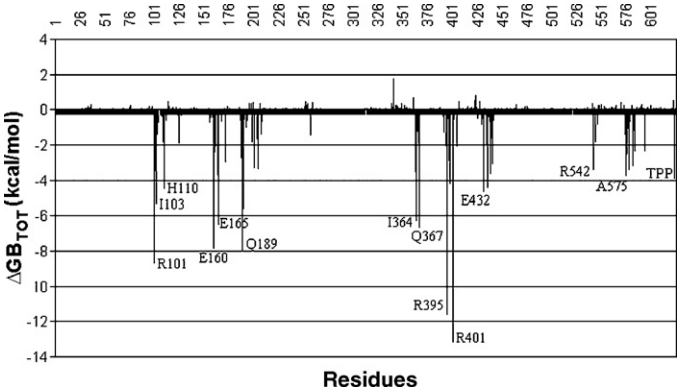

Fig. 9. MMGBSA 'per residue' decomposition, showing the molecular mechanics and solvation contributions to the dimer binding of each residue of monomer 1, adding also TPP (residue 624), the structural metal (residue 625) and the structural water shown in Fig. 10 (residue 626).

driven by small clusters or hot spots that play the major role in protein–protein recognition. Interestingly, the three most important residues are, once again, Arg 401, Arg 395 and Arg 101, thus corroborating the experimental results [14] and the abovementioned discussion. However, other residues are also involved in strong dimer interactions: Ile 103, His 110, Glu 160, Glu 165, Gln 189, Ile 364, Gln 367, Glu 432, Arg 542 and Ala 575. It should be noted that half of these residues are conserved with respect to the yeast Transketolase, showing that conserved residues are also important to maintain protein–protein recognition and not only to participate in catalysis. The cofactor also shows a favorable contribution to the dimer formation of −4 kcal/mol (Fig. 9), although this contribution is secondary with respect to the contribution of other residues (e.g. Arg 401 with −13 kcal/mol).

3.4. Interaction analysis of TPP and description of the active site

An interaction analysis of the TPP cofactor and its binding site was performed by extracting and examining eight structures of the human model production dynamics (at a ratio of 1 structure/200 ps). As was described for the arginine residues, hydrogen bond, van der Waals and electrostatic energies were calculated for the Transketolase cofactors. Table 3 and Fig. 10 summarize the most stable hydrogen bonds maintained between TPP and the protein. Fig. 10 also shows the residues involved in metal coordination.

Although TPP is placed between the two monomers of Transketolase, all the hydrogen bonds found, except for some

Table 3
Geometrical parameters of the hydrogen bond found between Transketolase and TPP throughout the simulation.

Transketolase	TPP	Average distance (Å)	Distance RMS (Å)	Average angle (°)	Angle RMS (°)
Gly 123 O	NH	3.5	0.7	110.4	16.6
Asn 185 ND2-HD21	O7	1.9	0.1	152.5	8.6
Lys 244 NZ-HZ2	O9	2.8	0.6	83.6	43.0
Thr 39 OG1-HG1	O9	1.7	0.1	158.2	8.3
His 77 ND1-HD1	O9	1.8	0.1	161.8	8.3
Ser 40 OG-HG	O8	1.7	0.1	164.9	7.2
Lys 75 NZ-HZ1	O8	1.9	0.1	139.9	9.8
Lys 75 NZ-HZ2	O10	1.8	0.1	162.4	9.0

The atom nomenclature for TPP can be seen in Fig. 10.

weak hydrogen bonds (not shown in Fig. 10), belong to one monomer. This is consistent with the analysis of other Transketolase variants, where one of the monomers participates in polar interactions with TPP (hydrogen bonds) while the other takes part in non-polar interactions [12]. The aminopyrimidine ring of TPP establishes weak hydrogen bonds, but the main interactions are focused on the pyrophosphate moiety, which maintains seven stable hydrogen bonds. His 77, which forms a hydrogen bond with the pyrophosphate, is a conserved residue that was also identified in the yeast variant as being involved in TPP binding [7–9].

Table 4 shows the distances of metal ion coordination. The metal ion is coordinated by two oxygen atoms of TPP, three residues (Asp 155, Asp 183 and Asn 185) and a structural water, also identified in yeast Transketolase [29]. As can be seen in Table 4, a small fluctuation is noticed in all atom-metal distances, in keeping with a strong metal coordination.

With respect to Asp 155, it has been suggested that this residue is involved in metal coordination in human Transketolase, and also that its mutation to alanine abolishes TPP binding and dimer formation [12]. This model demonstrates the role of Asp 155 in metal coordination. Moreover, McCool et al. [55] previously suggested, based on a sequence alignment, a role for Asp 183, Asp 155 and Asn 185 in metal coordination or TPP binding in the human protein, and our model confirms this.

Table 4
Metal coordination distances and deviations throughout the simulation.

Atoms	Average distance (Å)	Distance RMS (Å)
TPP O6	2.3	0.1
Structural water O	2.4	0.1
Asp 155 OD2	2.2	0.1
Asp 183 OD2	2.4	0.1
Asp 183 OD1	2.4	0.1
Asn 185 OD1	2.4	0.1
TPP O7	2.2	0.1

Nomenclature of the TPP atoms is shown in Fig. 10.

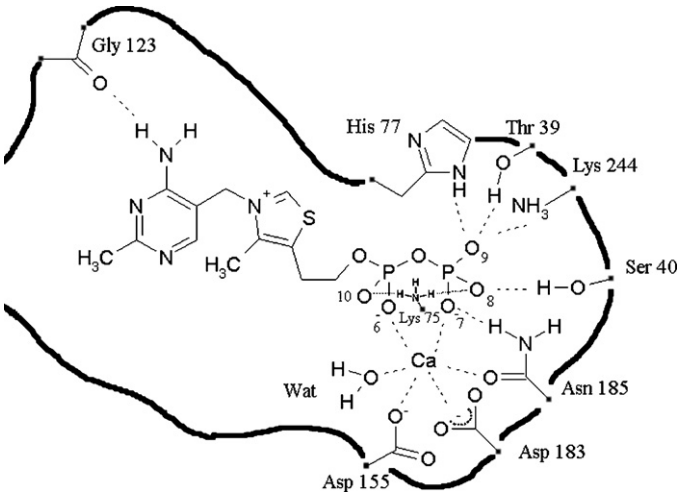

Fig. 10. Visual representation of hydrogen bond involved in the TPP binding to Transketolase. It is also shown the coordination of the metal ion. Most important interactions are remarked in dotted lines.

The hydrogen bond pattern and metal coordination are similar in the yeast protein and our model of human Transketolase [29], which also includes a structural water involved in metal binding.

As regards van der Waals and electrostatic interaction energies, the TPP cofactor was decomposed into ten representative chemical fragments (Fig. 11) in order to search for the most favorable intermolecular interactions with the model of human Transketolase. Average energies extracted from eight structures of the production dynamics are shown in Fig. 12A and B. As can be seen in Fig. 12A, the chemical fragments 2 and 5, which correspond to the aminopyrimidine and the thiazolium rings, respectively, show the most notable van der Waals energies (around −11 kcal/mol). Methyl groups of both rings contribute with lower energies. The aminopyrimidine fragment interacts tightly with Leu 125 (with an average energy of −7.2 kcal/mol), as well as with Phe 392 and Phe 389 of the other monomer (with average energies of −2.0 and −5.4 kcal/mol, respectively). These two phenylalanines are conserved residues that also interact with the cofactor in the yeast variant (equivalent to Phe 445 and Phe 442, respectively) [7–9], while Leu 125 was also suggested to interact with TPP in the human protein [55].

With respect to the thiazolium ring the most important contacts are maintained with conserved His 77 (average energy of −4.3 kcal/mol), which is equivalent to His 69 in the yeast variant, and with Tyr 363 of the other monomer (average energy of −1.9 kcal/mol). Conserved His 37 (equivalent to His 30 in the yeast variant) interacts slightly (average energy −0.6 kcal/mol), while non-conserved Gln 189 (equivalent to Ile 191) also maintains a contact with the thiazolium fragment (average energy −2.6 kcal/mol).

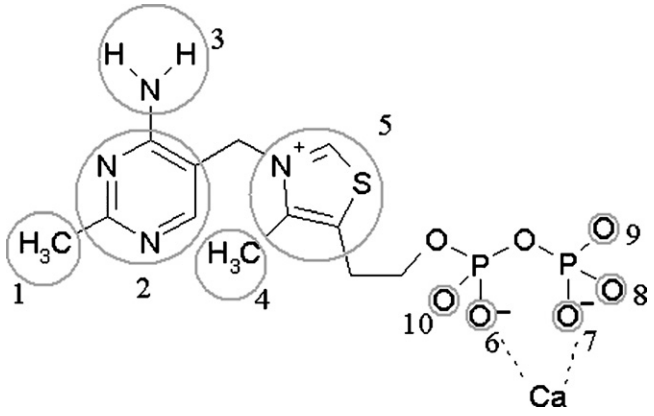

Fig. 11. Decomposition of TPP into chemical groups used for van der Waals and electrostatic analyses.

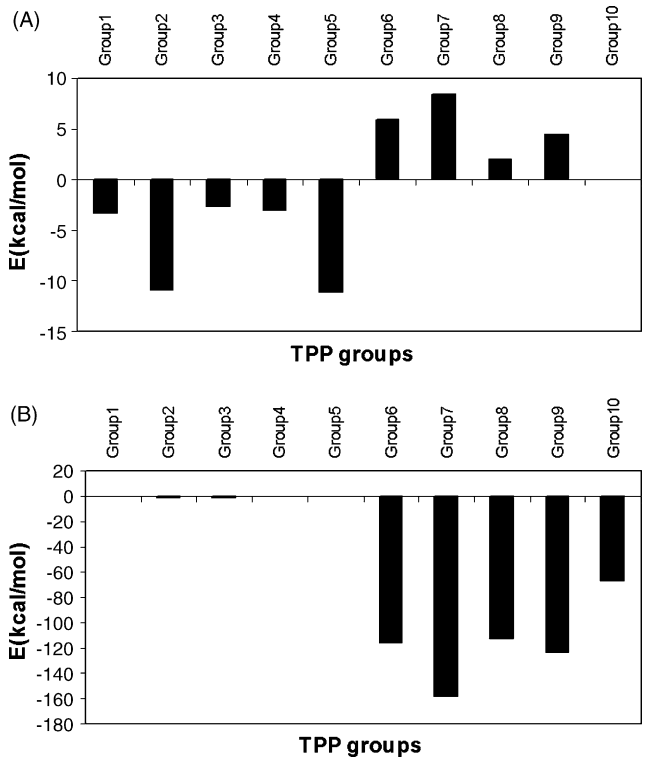

Fig. 12. (A) Average van der Waals interaction energies for chemical groups 1–10 of TPP and (B) average electrostatic interaction energies for chemical groups 1–10 of TPP.

These residues, His 30 and Ile 191, were found to be involved in TPP binding in the yeast Transketolase [7–9].

Surprisingly, no favorable van der Waals contacts were noticed in the pyrophosphate moiety and, moreover, positive values ranging from 5.0 to 9.0 kcal/mol were obtained. This aspect is solved as shown in Fig. 12B, where the high electrostatic energies of the pyrophosphate (groups 6–10) stabilize the bad van der Waals contacts. In line with the hydrogen bond analysis the pyrophosphate fragment maintains the most important interactions with the protein showing high electrostatic energies. The most important contact is maintained with O7 of the TPP cofactor, as this atom establishes two stable hydrogen bonds (with Ser 40 and Lys 75) and is also coordinated to the structural calcium ion. However, as pointed out above, the desolvation penalty of these groups could drastically reduce the final balance of electrostatic energy. The MMPB(GB)SA protocol, applied in the next section, can clarify this balance of van der Waals and electrostatic energies during the binding process.

The TPP binding site in the yeast variant is accessible from the solvent through a substrate channel [8,9] via which the reaction compounds reach the cofactor during catalysis. This channel is formed by a cluster of conserved histidine residues (His 30, His 69, His 103, His 263 and His 481) that are involved in substrate stabilization and proton transfer. Our model of the human protein also shows the substrate channel, involving the cluster of histidines, formed by His 37, His 77, His 110 and His 258 (equivalent to the first four histidines of the cluster in yeast) and Gln 428 from the other monomer (equivalent to His 481 in yeast). Moreover, the entrance to this channel is surrounded by conserved polar residues: Arg 101, Arg 474 from the other monomer, and Glu 423, also from the other monomer (equivalent to Arg 94, Arg 528 and Glu 476 in the yeast variant). Fig. 13 depicts the substrate channel shown in surface representation of the human model and these involved residues which have also been identified in the

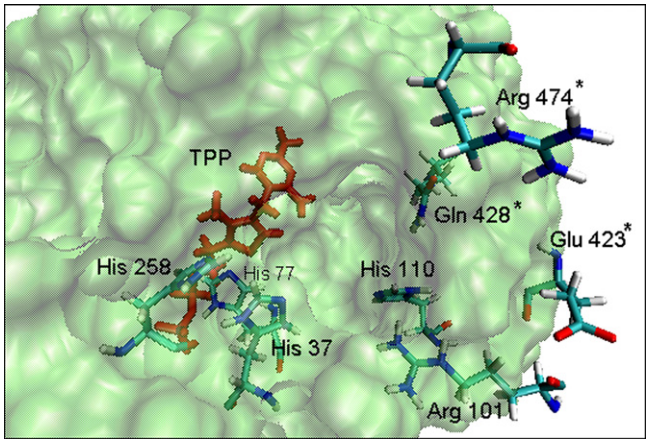

Fig. 13. Substrate channel found in the human model of Transketolase. TPP is remarked in red. The inner cluster of histidines (His 37, His 77, His 110 and His 258) and the residues located at the entrance of the channel (Arg 101, Glu 423 and Arg 474) are also shown. Asterisks denote for residues that belong to the monomer 2. Image created with the VMD software [34].

experimental structure of yeast Transketolase [7–9]. We suggest here that an interesting inhibitor could be a small molecule capable of interacting with residues located at the entrance to the substrate channel, thus blocking the natural substrates of Transketolase. In addition to the cofactor binding site and the substrate channel, we identified an extended hydrophobic site using Q-SiteFinder [56]. This new site has a volume of 680 $Å^3$ and is composed by three fragments of alpha helix (residues 132–139, 169–173 and 372–379), three fragments of beta sheet (residues 70–73, 149–151 and 174–179) and two loops (residues 140–148 and 232–236). Moreover this site is solvent accessible and therefore can be used in docking studies to find new human Transketolase inhibitors.

3.5. Binding free energy of TPP

As explained in Section 2 an MMPB(GB)SA protocol was applied to calculate the binding free energy of the TPP cofactor complexed with the human model of Transketolase. This methodology can complement the analysis of interactions discussed above adding quantitative energy contributions, such as electrostatic and van der Waals balances, solvation and entropic contributions. This section also aims to interpret the experimental results [22], which suggest a high favorable electrostatic energy for the complex between the protein and the cofactor. Thus, it has been shown that a simple molecule of pyrophosphate can compete with TPP for the binding site in the yeast variant, while a thiamine molecule cannot [22]. This is unusual because the hydrophobic forces are often the main contribution to the binding.

Table 5 shows the averaged results of the MMPB(GB)SA protocol. Different applications of this analysis were performed: the first (shown in the first column) was calculated by considering the ligand as the TPP molecule alone, while the second (shown in the second and third columns) was calculated by considering the ligand as the TPP molecule, the structural calcium and the structural water. Assignation of these structural fragments to the ligand itself or to the receptor is a matter of debate in the MMPB(GB)SA context [57], and so we have simulated and compared the two situations. As regards the entropic contribution, the metal ion and the structural water were assigned to the receptor in all cases.

In addition, the use of the parse radii set [39], first and second columns, or the bondi radii set [42], third column, is also discussed

Table 5
Binding free energy components, averaged over 100 snapshots, for TPP bound to the human Transketolase. ΔE_{ELE} and ΔE_{VDW} account for electrostatic and van der Waals in vacuo binding enthalpic contribution. ΔPB_{SUR} and ΔGB_{SUR} account for non-polar contribution to solvation using PB or GB, respectively, ΔPB_{CAL} and ΔGB_{CAL} are the polar contribution to solvation using PB or GB, respectively. ΔPB_{SOL} and ΔGB_{SOL} denote for the $\Delta PB_{SUR} + \Delta PB_{CAL}$ addition or the $\Delta GB_{SUR} + \Delta GB_{CAL}$ addition, respectively. ΔPB_{ELE} and ΔGB_{ELE} account for the $\Delta E_{ELE} + \Delta PB_{CAL}$ addition or $\Delta E_{ELE} + \Delta GB_{CAL}$ addition, respectively. ΔPB_{TOT} and ΔGB_{TOT} account for total enthalpic contribution, including the solvation, to the binding free energy, using PB or GB, respectively. $-T\Delta S_{TRAS}$ denotes for the translational entropic contribution, $-T\Delta S_{ROT}$ denotes for the rotational entropic contribution, $-T\Delta S_{VIB}$ accounts for the vibrational entropic contribution and $-T\Delta S_{TOT}$ accounts for the total entropic balance (all entropic components are calculated truncating the receptor to only those atom within a cutoff of 9 Å to the ligand and using 10 snapshots). Final theoretical free energy of binding at 300 K is denoted as ΔG_{MMPBSA} using the PB calculation or ΔG_{MMGBSA} using the GB calculation.

	Binding free energy components (kcal/mol)		
	Ligand = TPP parse radii	Ligand = TPP + Ca + Wat parse radii	Ligand = TPP + Ca + Wat bondi radii
ΔE_{ELE}	−961.99	−448.99	−448.99
ΔE_{VDW}	−30.99	−29.94	−29.94
ΔPB_{SUR}	−5.82	−5.82	−5.82
ΔPB_{CAL}	942.52	512.79	515.85
ΔPB_{SOL}	936.70	506.96	510.03
ΔPB_{ELE}	−19.47	63.79	66.83
ΔPB_{TOT}	−56.28	28.04	31.10
ΔGB_{SUR}	−6.51	−6.51	−6.51
ΔGB_{CAL}	843.84 (GB1)	375.47 (GB1)	387.42 (GB2)
ΔGB_{SOL}	837.33 (GB1)	368.96 (GB1)	380.91 (GB2)
ΔGB_{ELE}	−118.15 (GB1)	−73.53 (GB1)	−61.57 (GB2)
ΔGB_{TOT}	−155.64 (GB1)	−109.97 (GB1)	−98.02 (GB2)
$-T\Delta S_{TRAS}$	13.12	13.12	13.12
$-T\Delta S_{ROT}$	10.72	10.72	10.72
$-T\Delta S_{VIB}$	−4.55	−4.55	−4.55
$-T\Delta S_{TOT}$	19.30	19.30	19.30
ΔG_{MMPBSA}	−36.98	47.34	50.40
ΔG_{MMGBSA}	−155.64	−90.67	−78.72

here. Finally, two generalized born methodologies were applied, based on either the Tsui and Case [40] parameterization or on that of Onufriev et al. [41] (denoted as GB1 and GB2, respectively).

As can be seen, when assigning only TPP as the ligand, binding is almost directed by electrostatic forces considering the *in vacuo* contribution, there being a huge value for the electrostatic balance (ΔE_{ELE}) and a lower van der Waals contribution (ΔE_{VDW}). The pyrophosphate fragment of TPP is clearly correlated with the former contribution while the thiamine fragment is responsible for the latter contribution. However, as commented previously, this electrostatic energy is penalized with a high electrostatic solvation balance (ΔPB_{SOL} or ΔGB_{SOL}) to achieve a total polar contribution to the binding of −19.47 kcal/mol, using PB, and −118.15 kcal/mol when using GB. With respect to the entropic balance during binding, translational ($-T\Delta S_{TRAS}$) and rotational modes ($-T\Delta S_{ROT}$) are not favorable for binding, although vibrational entropic contribution ($-T\Delta S_{VIB}$) is favorable, adding −4.55 kcal/mol to the final binding free energy. The total entropic contribution decreases the binding free energy by 19.30 kcal/mol. A final binding free energy of −36.98 kcal/mol (ΔG_{MMPBSA}) or −155.64 kcal/mol (ΔG_{MMGBSA}) corroborates the high affinity of the cofactor. However, it should be noted that in this analysis it is more appropriate to consider relative rather than absolute energies, due to implicit limitations of the method and to simplifications in its application [58].

As regards the driving force of binding, the results using PB and GB are contradictory. The $\Delta E_{VDW} + \Delta PB_{SUR}$ addition (−36.81 kcal/mol) denotes the hydrophobic binding energy and it is more favorable than the polar contribution, $\Delta E_{ELE} + \Delta PB_{CAL}$ (−19.47 kcal/mol). Thus, TPP binding seems to be driven by van der Waals energy. However, when the same balance is considered using the GB framework the binding appears to be driven by electrostatic forces, in line with the experimental assays of yeast Transketolase [22]. Thus, $\Delta E_{VDW} + \Delta GB_{SUR}$ is −37.50 kcal/mol, while $\Delta E_{ELE} + \Delta GB_{CAL}$ is −118.15 kcal/mol.

However, it has been shown [59–63] that the PB methodology has certain limitations when dealing with charged ligands such as TPP, specifically, that it shows too high polar desolvation contributions (ΔPB_{CAL}), whereas this contribution is normalized for zwitterionic or neutral ligands. Thus, it seems more appropriate to describe TPP binding by means of the MMGBSA protocol.

As for the results using the second definition of the ligand (shown in the second column of Table 5), the *in vacuo* electrostatic balance (ΔE_{ELE}) is drastically reduced, since the structural water and the structural calcium are now part of the ligand and therefore their mutual interaction with TPP is not taken into account to calculate the final binding energies. For this reason, the polar contribution to the binding, adding $\Delta E_{ELE} + \Delta PB_{CAL}$ (63.8 kcal/mol), is now positive (binding unfavorable) and the binding is still driven by van der Waals forces. The MMGBSA once again predicts a binding driven by electrostatic forces, with the polar contribution $\Delta E_{ELE} + \Delta GB_{CAL}$ (−73.52 kcal/mol) being more favorable than the hydrophobic contribution $\Delta E_{VDW} + \Delta GB_{SUR}$ (−35.76 kcal/mol).

Finally, the results using the bondi radii set [42] and the parameterization of Onufriev et al. [41], denoted here as GB2, are shown in the third column of Table 5. These results are very similar with respect to the second alternative shown in the second column, and thus no additional information is added by changing the method and the set of radii applied to solve the polar contributions to solvation.

To conclude this section, assuming that the GB approach is better able to describe a highly charged molecule such as TPP, the most important binding interactions are electrostatic, in agreement with the proposed binding for the yeast Transketolase [22]. However, van der Waals and hydrophobic forces are also important for binding when using both approximations (especially for the MMPBSA protocol). In all cases the entropic factors are not a determining factor when describing binding.

4. Conclusions

This study has presented a homology model of human Transketolase in order to provide a reliable model with which to design new inhibitors and to investigate the role of some conserved residues between the yeast and human proteins. Despite the low sequence identity between the human protein and the yeast protein used as a template, the model does have

acceptable profiles for the three programs of structural analysis applied. In addition, the molecular dynamics simulation improved the general structure of the model and stable RMS deviations throughout the simulation were also obtained.

An accurate energetic analysis has been performed in order to demonstrate the role of five arginine residues: conserved Arg 101, Arg 318, Arg 401, Arg 474 and non-conserved Arg 395. Arg 401 (equivalent to Arg 433 in the rat variant) has been identified as an important residue that maintains the dimerization structure close to the cofactor binding site. We conclude that Arg 395 also makes a notable contribution to the dimer stability of the protein. The study has also described the cofactor (thiamine pyrophosphate), its binding site and its substrate channel, revealing similarities with respect to the yeast variant and corroborating some predictions made for the human variant. The coordination of the structural cation has also been discussed, showing a structural water which was also found in the yeast variant. In this context the model confirmed the role of Asp 155, Asp 183 and Asn 185 in metal coordination and cofactor stability. Finally, an MMPB(GB)SA protocol was applied to calculate additional quantitative results for the description of cofactor binding. Different calculations were made by changing the definition of the ligand to include the structural calcium and the structural water, as well as by applying two alternative GB frameworks.

The main binding forces were identified and shown to corroborate the experimental results, assuming the better performance of MMGBSA for describing charged ligands.

In the absence of the experimental structure of human Transketolase we hope that our model will be useful to design new inhibitors that could bind to the proposed critical sites. Work in this context is in progress.

Acknowledgements

The Spanish Ministry of Science and Technology supported this work through the project CTQ2006-06588/BQU. We are also grateful to the 'Departament d'Universitats, Recerca i Societat de la informació de la Generalitat de Catalunya i del Fons Social Europeu'.

References

[1] B. Comín-Anduix, J. Boren, S. Martinez, C. Moro, J.J. Centelles, R. Trebukhina, N. Petushok, W.N. Lee, L.G. Boros, M. Cascante, The effect of thiamine supplementation on tumour proliferation. A metabolic control analysis study, Eur. J. Biochem. 268 (2001) 4177–4182.
[2] M. Héroux, V.L. Raghavendra Rao, J. Lavoie, J.S. Richardson, R.F. Butterworth, Alterations of thiamine phosphorylation and of thiamine-dependent enzymes in Alzheimer's disease, Metab. Brain Dis. 11 (1996) 81–88.
[3] D.S. Shreve, M.P. Holloway, J.C. Haggerty III, H.Z. Sable, The catalytic mechanism of Transketolase. Thiamin pyrophosphate-derived transition states for Transketolase and pyruvate dehydrogenase are not identical, J. Biol. Chem. 258 (1993) 12405–12408.
[4] A. Schellenberger, Thiamin pyrophosphate binding mechanism and the function of the aminopyrimidine part, J. Nutr. Sci. Vitaminol. (1992) 392–396, Spec No.
[5] L.G. Boros, J. Puigjaner, M. Cascante, W.N. Lee, J.L. Brandes, S. Bassilian, F.I. Yusuf, R.D. Williams, P. Muscarella, W.S. Melvin, W.J. Schirmer, Oxythiamine and dehydroepiandrosterone induce a G1 phase cycle arrest in Ehrlich's tumor cells through inhibition of the pentose cycle, FEBS Lett. 456 (1999) 113–118.
[6] U. Nilsson, Y. Lindqvist, Ro. Kluger, G. Schneider, Crystal structure of Transketolase in complex with thiamine thiazolone diphosphate, an analogue of the reaction intermediate, at 2.3 Å resolution, FEBS Lett. 326 (1993) 145–148.
[7] C. Wikner, U. Nilsson, L. Meshalkina, C. Udekwu, Y. Lindqvist, G. Schneider, Identification of catalytically important residues in yeast Transketolase, Biochemistry 36 (1997) 15643–15649.
[8] Y. Lindqvist, G. Schneider, U. Ermler, M. Sündstrom, Three-dimensional structure of Transketolase, a thiamine diphosphate dependent enzyme, at 2.5 Å resolution, EMBO J. 11 (1992) 2373–2379.
[9] M. Nikkola, Y. Lindqvist, G. Schneider, Refined structure of transketolase from *Saccharomyces cerevisiae* at 20 Å resolution, J. Mol. Biol. 238 (1994) 387–404.
[10] M.N. Isupov, M.P. Rupprecht, K.S. Wilson, Z. Dauter, J.A. Littlechild, Crystal Structure of *Escherichia coli* Transketolase, in press.
[11] S. Gerhardt, S. Echt, M. Busch, J. Freigang, G. Auerbach, G. Bader, W.F. Martin, A. Bacher, R. Huber, M. Fischer, Structure and properties of an engineered Transketolase from maize, Plant Physiol. 132 (2003) 1941–1949.
[12] J.J. Wang, P.R. Martin, C.K. Singleton, Aspartate 155 of human Transketolase is essential for thiamine diphosphate-magnesium binding, and cofactor binding is required for dimer formation, Biochim. Biophys. Acta 1341 (1997) 165–172.
[13] M.X. Du, J. Sim, L. Fang, Z. Yin, S. Koh, J. Stratton, J. Pons, J.J. Wang, B. Carte, Identification of novel small-molecule inhibitors for human Transketolase by high-throughput screening with fluorescent intensity (FLINT) assay, J. Biomol. Screen. 9 (2003) 427–433.
[14] Y. Soh, B.J. Song, J. Jeng, A.T. Kallarakal, Critical role of arg433 in rat Transketolase activity as probed by site-directed mutagenesis, Biochem. J. 333 (1998) 367–372.
[15] A.A. Thomas, J. De Meese, Y. Le Huerou, S.A. Boyd, T.T. Romoff, S.S. Gonzales, I. Gunawardana, T. Kaplan, F. Sullivan, K. Condroski, J.P. Lyssikatos, T.D. Aicher, J. Ballard, B. Bernat, W. DeWolf, M. Han, C. Lemieux, D. Smith, S. Weiler, S.K. Wright, G. Vigers, B. Brandhuber, Non-charged thiamine analogs as inhibitors of enzyme Transketolase, Bioorg. Med. Chem. Lett. 18 (2008) 509–512.
[16] A.A. Thomas, Y. Le Huerou, J. De Meese, I. Gunawardana, T. Kaplan, T.T. Romoff, S.S. Gonzales, K. Condroski, S.A. Boyd, J. Ballard, B. Bernat, W. DeWolf, M. Han, P. Lee, C. Lemieux, R. Pedersen, J. Pheneger, G. Poch, D. Smith, F. Sullivan, S. Weiler, S.K. Wright, J. Lin, B. Brandhuber, G. Vigers, Synthesis, in vitro and in vivo activity of thiamine antagonist Transketolase inhibitors, Bioorg. Med. Chem. Lett. 18 (2008) 2206–2210.
[17] Y. Le Huerou, I. Gunawardana, A.A. Thomas, S.A. Boyd, J. de Meese, W. Dewolf, S.S. Gonzales, M. Han, L. Hayter, T. Kaplan, C. Lemieux, P. Lee, J. Pheneger, G. Poch, T.T. Romoff, F. Sullivan, S. Weiler, S.K. Wright, J. Lin, Prodrug thiamine analogs as inhibitors of the enzyme Transketolase, Bioorg. Med. Chem. Lett. 18 (2008) 505–508.
[18] Z. Zhou, M. Bates, J.D. Madura, Structure modeling, ligand binding, and binding affinity calculation (LR-MM-PBSA) of human heparanase for inhibition and drug design, Proteins 65 (2006) 580–592.
[19] P. Aparoy, R.N. Reddy, L. Guruprasad, M.R. Reddy, P. Reddanna, Homology modeling of 5-lipoxygenase and hints for better inhibitor design, J. Biomol. Screen. 9 (2004) 5427–5433.
[20] M. Li, B. Wang, Homology modeling and examination of the effect of the D92E mutation on the N5H1 nonstructural protein NS1 effector domain, J. Mol. Model. 13 (2007) 1237–1244.
[21] P.A. Kollman, I. Massova, C. Reyes, B. Kuhn, S. Huo, L. Chong, M. Lee, T. Lee, Y. Duan, W. Wang, O. Donini, J. Srivasan, D.A. Case, T.E. Cheatam III, Calculating structures and free energies of complex molecules: combining molecular mechanics and continuum models, Acc. Chem. Res. 33 (2000) 889–897.
[22] A. Schellenberger, Sixty years of thiamin diphosphate biochemistry, Biochim. Biophys. Acta 1385 (1998) 177–186.
[23] N. Eswar, M.A. Mari-Renom, B. Webb, M.S. Madhusudhan, D. Eramian, M. Shen, U. Pieper, S. Sali, Comparative protein structure modeling with MODELLER, Curr. Protoc. Bioinformatics, 2006, Chapter 5, Unit 5.6.
[24] A. Sali, T.L. Blundell, Comparative protein modelling by satisfaction of spatial restraints, J. Mol. Biol. 234 (1993) 779–815.
[25] A. Fiser, R.K. Do, A. Sali, Modeling of loops in protein structures, Protein Sci. 9 (2000) 1753–1773.
[26] M. Sundström, Y. Lindqvist, G. Schneider, U. Hellman, H. Ronne, Yeast TKL1 gene encodes a Transketolase that is required for efficient glycolysis and biosynthesis of aromatic amino acids, J. Biol. Chem. 268 (1993) 24346–24352.
[27] M. Heinig, D. Frishman, STRIDE: a web server for secondary structure assigment from known atomic coordinates of proteins, Nucleic Acids Res. 32 (2004) W500–W502.
[28] D.A. Case, D.A. Pearlman, J.W. Caldwell, T.E. Cheathan III, J. Wang, W.S. Ross, C.L. Simmerling, T.D. Darden, K.M. Merz, R.V. Stanton, A.L.Cheng, J.J. Vincent, M. Crowley, V. Tsui, H. Gohlke, R.J. Radmer, Y. Duan, J. Pitera, I. Massova, G.L. Seibel, U.C. Sligh, P.K. Weiner, P.A. Kollman, AMBER 7, Univ. California, San Francisco, 2002.
[29] G.A. Kochetov, Functional flexibility of the Transketolase molecule, Biochemistry 66 (2001) 1077–1085.
[30] J. Wang, R.M. Wolf, J.W. Caldwell, P.A. Kollman, D.A. Case, Development and testing of a general amber force field, J. Comput. Chem. 26 (2005) 114.
[31] M.J. Frisch, G.W. Trucks, H.B. Schlegel, G.E. Scuseria, M.A. Robb, J.R. Cheeseman, V.G. Zakrzewski, J.A. Montgomery Jr., R.E. Stratmann, J.C. Burant, S. Dapprich, J.M. Millam, A.D. Daniels, K.N. Kudin, M.C. Strain, O. Farkas, J. Tomasi, V. Barone, M. Cossi, R. Cammi, B. Mennucci, C. Pomelli, C. Adamo, S. Clifford, J. Ochterski, G.A. Petersson, P.Y. Ayala, Q. Cui, K. Morokuma, D.K. Malick, A.D. Rabuck, K. Raghavachari, J.B. Foresman, J. Cioslowski, J.V. Ortiz, A.G. Baboul, B.B. Stefanov, G. Liu, A. Liashenko, P. Piskorz, I. Komaromi, R. Gomperts, R.L. Martin, D.J. Fox, T. Keith, M.A. Al-Laham, C.Y. Peng, A. Nanayakkara, C. Gonzalez, M. Challacombe, P.M.W. Gill, B. Johnson, W. Chen, M.W. Wong, J.L. Andres, M. Head-Gordon, E.S. Replogle, J.A. Pople, Gaussian 98. Revision A.6, Gaussian, Inc., Pittsburgh, PA, 1998.
[32] T. Darden, D. York, L. Pedersen, Particle mesh Ewald: an W log(N) method for Ewald sums in large systems, J. Chem. Phys. 98 (1993) 10089–10092.
[33] W.D. Cornell, P. Cieplak, C.I. Bayly, I.R. Goud, K.M. Mertz Jr., D.M. Ferguson, D.C. Spellmeyer, T. Fox, J.W. Caldwell, P.A. Kollman, A second generation of force fields for the simulation of proteins, nucleic acids and organic molecules, J. Am. Chem. Soc. 117 (1995) 5179–5197.
[34] W. Humprey, A. Dalke, K. Schulten, VMD-visual molecular dynamics, J. Mol. Graph. 14 (1996) 33–38.
[35] E.F. Pettersen, T.D. Goddard, C.C. Huang, G.S. Couch, D.M. Greenblatt, E.C. Meng, T.E. Ferrin, UCSF Chimera—a visualization system for exploratory research and analysis, J. Comput. Chem. 25 (2004) 1605–1612.

[36] H.J.C. Berendsen, J.P.M. Postman, W.F. Van Gunsteren, A. DiNola, J.A. Haak, Molecular dynamics with coupling to an external bath, J. Chem. Phys. 81 (1984) 3684–3690.
[37] J.P. Ryckaert, G. Ciccotti, H.J. Berendsen, Numerical integration of the Cartesian equations of motion of a system with constraints: molecular dynamics of *n*-alkanes, J. Comput. Chem. 23 (1977) 327–341.
[38] D. Bashford, K. Gerwent, Electrostatic calculations of the pK_a values of ionizable groups in bacteriorhodopsin, J. Mol. Biol. 224 (1992) 473–486.
[39] D. Sitkoff, K. Sharp, B. Honing, Accurate calculations of hydration free energies using macroscopic solvents, J. Phys. Chem. 98 (1994) 1978–1988.
[40] V. Tsui, D.A. Case, Theory and applications of the generalized born solvation model in macromolecular simulations, Nucleic Acids Sci. 56 (2001) 275–291.
[41] A. Onufriev, D. Bashford, D.A. Case, Generalized Born models of macromolecular solvation effects, Annu. Rev. Phys. Chem. 51 (2000) 129–152.
[42] A. Bondi, VDW volumes and radii, J. Phys. Chem. 68 (1964) 441–451.
[43] J. Weiser, P.S. Shemkin, W.C. Still, Approximate atomic surfaces from linear combinations of pairwise overlaps (LCPO), J. Comput. Chem. 20 (1999) 217–230.
[44] R.A. Laskowski, M.W. MacArthur, D.S. Moss, J.M. Thornton, PROCHECK: a program to check the stereochemical quality of protein structures, J. Appl. Cryst. 26 (1993) 283–291.
[45] D. Eisenberg, R. Luthy, J.U. Bowie, VERIFY3D: assessment of protein models with three-dimensional profiles, Methods Enzymol. 277 (1997) 396–404.
[46] M. Wiederstein, M.J. Sippl, ProSA-Web: interactive web service for the recognition of errors in three-dimensional structures of proteins, Nucleic Acids Res. 35 (2007) 407–410.
[47] Z. Hu, B. Ma, H. Wolfson, R. Nussinov, Conservation of polar residues as hot spots at protein interfaces, Proteins 39 (2000) 331–334.
[48] A.B. Kremer, R.M. Egan, H.Z. Sable, The active site of Transketolase. Two arginine residues are essential for activity, J. Biol. Chem. 255 (1980) 2405–2410.
[49] P.L. Masic, Arginine mimetic structures in biologically active antagonists and inhibitors, Curr. Med. Chem. 13 (2006) 3627–3648.
[50] J. Dumond, N. Boggetto, H.J. Schramm, W. Schramm, M. Takahashi, M. Reboud-Ravaux, Thyroxine-derivatives of lipopeptides: bifunctional dimerization inhibitors of human immunodeficiency virus-1 protease, Biochem. Pharmacol. 65 (2003) 1097–1102.
[51] P. Breccia, N. Boggetto, R. Pérez-Fernández, M. Van Gool, M. Takahashi, L. René, P. Prados, B. Badet, M. Reboud-Ravaux, J. de Mendoza, Dimerization inhibitors of HIV-1 protease based on a bicyclic guanidinium subunit, J. Med. Chem. 46 (2003) 5196–5207.
[52] U. Nilsson, C. Meshalkina, Y. Cindqvist, G. Schneider, Examination of substrate binding in thiamin diphosphate-dependent Transketolase by protein crystallography and site-directed mutagenesis, J. Biol. Chem. 272 (1997) 1864–1869.
[53] E. Jacoby, Biphenyls as potential mimetics of α-Helix, Bioorg. Med. Chem. Lett. 12 (2002) 891–893.
[54] H. Gohlke, Ch. Kiel, D.A. Case, Insights into protein–protein binding by binding free energy calculation and free energy decomposition for Ras–Raf and Ras–RalGDS complexes, Mol. Biol. 330 (2003) 891–913.
[55] B.A. McCool, S.G. Plonk, P.R. Martins, C.K. Singleton, Cloning of human Transketolase cDNAs and comparison of the nucleotide sequence of the coding region in Wernicke-Korsakoff and non-Wernicke-Korsakoff individuals, J. Biol. Chem. 268 (1993) 1397–1404.
[56] A.T. Laurie, R.M. Jackson, Q-SiteFinder: an energy-based method for the prediction of protein-ligand binding sites, Bioinformatics 21 (2005) 1908–1916.
[57] N. Spackova, T.E. Cheatham, F. Ryjacek, F. Lankas, L. van Meervelt, P. Hobza, J. Sponer, Molecular dynamics simulations and thermodynamics analysis of DNA-drug complexes. Minor groove binding between 4′,6′-diamidino-2-phenylindole and DNA duplexes in solution, J. Am. Chem. Soc. 125 (2003) 1759–1769.
[58] D.A. Pearlman, Evaluating the molecular mechanics Poisson–Boltzmann surface area free energy method using a cogeneric series of ligands to p38 MAP kinase, J. Med. Chem. 48 (2005) 7796–7806.
[59] P. Bonnet, R.A. Bryce, Scoring binding affinity of multiple ligands using implicit solvent and a single molecular dynamics trajectory: application to influenza neuraminidase, J. Mol. Graph. Model. 24 (2005) 147–156.
[60] P. Bonnet, R.A. Bryce, Molecular dynamics and free energy analysis of neuraminidase–ligand interactions, Protein Sci. 13 (2004) 946–957.
[61] B.J. Smith, P.M. Colman, M. von Itzstein, B. Daylec, J.N. Varghese, Analysis of inhibitor binding in influenza virus neuraminidase, Protein Sci. 10 (2001) 689–696.
[62] N.R. Taylor, M. von Itzstein, A structural and energetics analysis of the binding of a series of *N*-acetylneuraminic-acid-based inhibitors to influenza virus sialidase, J. Comput. Aided Mol. Des. 10 (1996) 233–246.
[63] C. Obiol-Pardo, J. Rubio-Martinez, Comparative evaluation of MMPBSA and XSCORE to compute binding free energy in XIAP-peptide complexes, J. Chem. Inform. Model. 47 (2007) 134–142.